Optical Entanglement Facilitated by Opto-Mechanical Cooling

Alexandr V. Karpenko, Andrey B. Matsko, and Sergey P. Vyatchanin 1, 3, 4

¹Faculty of Physics, M.V. Lomonosov Moscow State University, Leninskie Gory, Moscow 119991, Russia

²Jet Propulsion Laboratory, California Institute of Technology,

4800 Oak Grove Drive, Pasadena, California 91109-8099, USA

³Quantum Technology Centre, M.V. Lomonosov Moscow State University, Leninskie Gory, Moscow 119991, Russia

⁴Faculty of Physics, Branch of M.V. Lomonosov Moscow State University in Baku,

1 Universitet street, Baku, AZ1144, Azerbaijan

(Dated: November 24, 2025)

Optomechanical generation of entangled optical beams is usually hindered by thermal noise. We present a theoretical study of low frequency entanglement generation between two nondegenerate optical harmonics emitted from a cavity optomechanical system operating in the resolved-sideband regime. The system comprises three nearly equidistant optical modes in a high-finesse Fabry–Perot cavity, with the central mode coherently driven. This configuration enables radiation-pressure interactions that generate strong quantum correlations between the two undriven sideband modes. Remarkably, these correlations persist even at large numbers of thermal phonons if one properly engineers the optical cooling rate of the mechanical mode. Entanglement is verified using a full quantum Langevin model that accounts for thermal noise and optical losses. Our findings demonstrate the feasibility of robust entanglement under ambient conditions, opening new avenues for hybrid quantum technologies based on mechanical interfaces and continuous-variable quantum information processing. ©2025 All Rights Reserved.

I. INTRODUCTION

Entanglement is one of the most profound and nonclassical features of quantum mechanics, and it has played a central role in discussions of the foundations of physics since the early work of Einstein, Podolsky, and Rosen (EPR) [1]. Their seminal argument, pointing to the apparent incompleteness of quantum theory, motivated decades of research into the nature of quantum correlations. Schrodinger subsequently coined the term "entanglement" to emphasize its fundamental significance [2]. The development of Bell's inequalities [3] and their experimental violation [4–6] established entanglement as a genuine physical phenomenon rather than a paradoxical artifact. Today, entanglement is understood not only as a signature of nonlocality, but also as a resource enabling quantum communication, quantum computation, and precision metrology [7].

In parallel with these conceptual advances, continuous-variable (CV) entanglement has emerged as a practical framework for implementing quantum information protocols using quadrature-amplitude correlations of bosonic modes of light and matter [8]. The Duan–Simon inseparability criterion [9, 10] and the Reid EPR criterion for inferred variances [11] provided experimentally testable conditions to verify CV entanglement. Since then, entangled optical beams have been generated using parametric down-conversion [12], four-wave mixing [13], and atomic ensembles [14], leading to demonstrations of quantum teleportation, dense coding, and quantum-enhanced sensing.

More recently, cavity optomechanics has emerged as a powerful platform for studying CV entanglement at the interface of light and matter [15]. In such systems, the quantized radiation pressure force couples optical fields

to the motion of a mechanical element, enabling a wide range of nonlinear quantum phenomena. Optomechanical interactions can, in principle, mediate entanglement between mechanical and optical modes [16], between multiple mechanical oscillators [17–19], and between distinct optical channels [20, 21]. This versatility makes optomechanics a natural candidate for hybrid quantum networks that combine disparate degrees of freedom, and for CV quantum information protocols operating at telecom or microwave frequencies.

Experimental progress has already demonstrated squeezed light from optomechanical cavities [22–24] and even entanglement between distant mechanical oscillators mediated by light [18, 19]. However, realizing robust and stationary entanglement between multiple optical harmonics mediated by a mechanical degree of freedom remains challenging, particularly under ambient conditions. The central difficulty is the omnipresent thermal noise that populates mechanical resonators. Thermal fluctuations act as an effective decoherence channel, washing out quantum correlations and suppressing entanglement [15, 16]. For this reason, most experimental demonstrations of optomechanical entanglement have required cryogenic environments, high-quality mechanical oscillators, or active reservoir engineering [25, 26].

Several strategies have been proposed to mitigate thermal decoherence. These include pulsed optomechanical protocols, where transient entanglement is generated faster than the thermalization timescale [26, 27]; reservoir engineering techniques that shape optical dissipation channels to stabilize entangled steady states [21, 25]; and hybrid approaches involving reservoir engineering [28]. Nonetheless, achieving steady-state entanglement between two propagating optical modes at large numbers of thermal phonons, without auxiliary cryogenics or

feedback, remains an outstanding challenge.

In this work, we address this challenge by studying theoretically a three-mode Fabry-Perot cavity system operating in the resolved-sideband regime. The cavity has one of the mirrors movable with the free motion having properties of a linear harmonic oscillator. The system includes three nearly equidistant optical resonances (with frequencies ω_+ , ω_0 , and ω_-), with ω_0 by frequency of the central mode (ω_0) coherently driven by an external laser. Frequencies ω_{\pm} are separated from ω_0 by frequency ω_m of mechanical oscillator: $\omega_{\pm} = \omega_0 \pm \omega_m$. Radiation pressure couples the driven mode to a mechanical oscillator, and through this interaction generates strong quantum correlations between the two undriven sideband modes. Remarkably, we show that by properly engineering the optical cooling rate of the mechanical oscillator, the quantum correlations persist even in the presence of strong thermal noise. Using a full quantum Langevin treatment that incorporates both optical losses and thermal decoherence, we demonstrate that the output sideband modes can become entangled under realistic parameters. Our results highlight the feasibility of generating robust CV entanglement of optical beams in ambient conditions, thereby paving the way for practical optomechanical interfaces for quantum communication, sensing, and information processing.

We analyze the generation of entanglement between the output optical fields associated with the sideband modes ω_{\pm} . This entanglement originates from the optomechanical interaction between the cavity field and the mechanical oscillator. A substantial degree of entanglement can be achieved when two conditions are satisfied. First, the thermal noise of the mechanical oscillator must be strongly suppressed, such that the average number of thermal phonons is reduced to $n_T \ll 1$. This suppression can be realized through optical damping, which arises from the asymmetry of the optomechanical coupling to the sideband modes ω_{\pm} . Second, the optical pump driving the central cavity mode ω_0 must be sufficiently strong to enhance the effective nonlinear interaction between the optical fields and the mechanical motion.

Experimental verification of this entanglement requires separation of the output light corresponding to the modes ω_{\pm} . However, direct spectral discrimination is extremely challenging, since the frequency difference $\omega_{+}-\omega_{-}$ is negligibly small on the optical scale. To circumvent this limitation, we propose the use of synodyne detection [29]. In this approach, the combined output from all three modes, ω_0 and ω_{\pm} , is directed to a balanced homodyne detector, while the local oscillator is prepared with two carrier frequencies, ω_{+} and ω_{-} . By adjusting the relative amplitudes and phases of these two frequency components of the local oscillator, it is possible to select arbitrary weighted combinations of quadratures. This capability provides the necessary measurement flexibility to reveal the presence of entanglement between the optical sidebands. Our results indicate that, under realistic experimental conditions, the proposed detection scheme enables direct observation of optomechanical entanglement between the sideband modes ω_{\pm} .

II. RESULTS

A. Hamiltonian

The unitary part of the system under study is governed by the canonical interaction Hamiltonian $H_{\rm int} \sim (E_0 + E_+ + E_-)^2 x$, where E_0 , E_- , and E_+ are the electric fields of the modes 0, -, and + on the surface of the moving mirror of a Fabry–Perot resonator. Within the rotating wave approximation, the Hamiltonian of the system can be written as

$$H = H_0 + H_{\text{int}},$$

$$H_0 = \hbar \omega_+ \hat{c}_+^{\dagger} \hat{c}_+ + \hbar \omega_0 \hat{c}_0^{\dagger} \hat{c}_0 + \hbar \omega_- \hat{c}_-^{\dagger} \hat{c}_- + \hbar \omega_m \hat{d}^{\dagger} \hat{d},$$

$$H_{\text{int}} = -i\hbar \left(\left[\eta_- \hat{c}_0^{\dagger} \hat{c}_- + \eta_+ \hat{c}_+^{\dagger} \hat{c}_0 \right] \hat{d} - adj. \right)$$

Here \hbar is the Planck constant. The term H_0 represents the free Hamiltonian describing the energies of the optical modes and the mechanical oscillator. The operators \hat{c}_0 , \hat{c}_0^{\dagger} , \hat{c}_{\pm} , and \hat{c}_{\pm}^{\dagger} denote the annihilation and creation operators corresponding to the optical modes, while \hat{d} and \hat{d}^{\dagger} are the annihilation and creation operators associated with the mechanical mode. The position operator \hat{x} of the mechanical oscillator is expressed as

$$\hat{x} = x_0 \left(\hat{d} + \hat{d}^{\dagger} \right), \quad x_0 = \sqrt{\frac{\hbar}{2m\omega_m}},$$
 (2.1)

where m is the effective mass of the oscillator and ω_m is its mechanical resonance frequency. The interaction term $H_{\rm int}$ represents the optomechanical coupling Hamiltonian. In this analysis, we consider a non-symmetric coupling configuration and introduce distinct coupling constants $\eta_{\pm} \sim x_0 \omega_0 / L$, where L denotes the effective length of the cavity. The asymmetry of the coupling constants come from the different mode geometry. Without loss of generality we consider real coupling constants in what follows.

B. Langevin equations

We denote the input optical field amplitudes by \hat{a}_{\pm} and \hat{a}_{0} . Using the Hamiltonian, we derive the corresponding Heisenberg–Langevin equations of motion for the slowly varying intracavity field amplitudes. These equations describe the temporal evolution of the optical and mechanical modes within the resonator:

$$\dot{\hat{c}}_0 + \gamma_0 \hat{c}_0 = \eta_+ \hat{c}_+ \hat{d}^\dagger - \eta_- \hat{c}_- \hat{d} + \sqrt{2\gamma_0} \,\hat{a}_0,$$
 (2.2a)

$$\dot{\hat{c}}_{+} + \gamma_{+} \hat{c}_{+} = -\eta_{+} \hat{c}_{0} \hat{d} + \sqrt{2\gamma_{+}} \, \hat{a}_{+}, \tag{2.2b}$$

$$\dot{\hat{c}}_{-} + \gamma_{-} \hat{c}_{-} = \eta_{-} \hat{c}_{0} \hat{d}^{\dagger} + \sqrt{2\gamma_{-}} \,\hat{a}_{-} \tag{2.2c}$$

$$\dot{\hat{d}} + \gamma_m \hat{d} = \eta_- \hat{c}_-^{\dagger} \hat{c}_0 + \eta_+ \hat{c}_0^{\dagger} \hat{c}_+ + \sqrt{2\gamma_m} \,\hat{q}. \tag{2.2d}$$

The coupling rates for the front mirror of the Fabry-Perot cavity are γ_{\pm} and γ_{0} . Operator \hat{q} corresponds to the stochastic Langevin force acting on the mechanical oscillator. The input noise operators \hat{a}_{\pm} and the thermal force operator \hat{q} are characterized by the following commutation and correlation relations:

$$\left[\hat{a}_{\pm}(t), \hat{a}_{\pm}^{\dagger}(t')\right] = \left\langle \hat{a}_{\pm}(t) \, \hat{a}_{\pm}^{\dagger}(t') \right\rangle = \delta(t - t'), \quad (2.3a)$$

$$\left[\hat{q}(t), \hat{q}^{\dagger}(t')\right] = \delta(t - t'), \tag{2.3b}$$

$$\langle \hat{q}(t)\hat{q}^{\dagger}(t')\rangle = (2n_T + 1)\,\delta(t - t'), \qquad (2.3c)$$

$$n_T = \left(e^{\hbar\omega_m/\kappa_B T} - 1\right)^{-1}.$$

Here, $\langle \dots \rangle$ denotes ensemble averaging. The parameter n_T is the thermal occupation number of the mechanical oscillator, κ_B is the Boltzmann constant, and T is the ambient temperature. The above relations assume Markovian reservoirs and describe the quantum and thermal noise entering the system through both optical and mechanical channels.

The coupling between the intracavity fields and the external optical modes is governed by the standard input–output boundary conditions:

$$\hat{b}_{\pm} = -\hat{a}_{\pm} + \sqrt{2\gamma_{\pm}}\hat{c}_{\pm},$$
 (2.4)

where \hat{b}_{\pm} are the output field operators corresponding to the reflected optical waves.

To facilitate further analysis, it is convenient to separate the steady-state (mean) components of the field amplitudes at the carrier frequency ω_0 from their small quantum fluctuations. Denoting the mean values by capital letters and the fluctuations by lowercase letters, we write

$$\hat{c}_0 \Rightarrow C_0 + c_0, \tag{2.5}$$

where C_0 represents the steady-state expectation value of the intracavity field amplitude in the central optical mode, while c_0 accounts for its quantum fluctuations. The assumption $|C_0|^2 \gg \langle c_0^{\dagger} c_0 \rangle$ ensures that the fluctuations are small compared to the mean field. Analogous decompositions can be introduced for the sideband optical modes and the mechanical mode. The amplitudes are normalized such that $\hbar \omega_0 |A_0|^2$ corresponds to the optical power of the incident wave [30].

In the following analysis, we assume that the steadystate amplitudes are real quantities:

$$A_0 = A_0^*, \quad C_0 = C_0^* = \sqrt{\frac{2}{\gamma_0}} A_0.$$
 (2.6)

This choice simplifies the analytical treatment and does not affect the generality of the results, as any phase factors can be absorbed into the definitions of the optical field operators.

C. Output fluctuations

To analyze the system dynamics, the differential equations are solved using the Fourier transform technique. In this treatment, we neglect the influence of the initial conditions and restrict our consideration to the stimulated response of the operators. The Fourier transform of a representative operator, such as \hat{a}_{\pm} , is introduced as

$$\hat{a}_{\pm}(t) = \int_{-\infty}^{\infty} a_{\pm}(\Omega), e^{-i\Omega t}, \frac{d\Omega}{2\pi}.$$
 (2.7)

The Fourier components $a_{\pm}(\Omega)$ satisfy the standard bosonic commutation and correlation relations,

$$\left[a_{\pm}(\Omega), a_{\pm}^{\dagger}(\Omega')\right] = 2\pi \,\delta(\Omega - \Omega'),\tag{2.8a}$$

$$\left\langle a_{\pm}(\Omega)a_{\pm}^{\dagger}(\Omega')\right\rangle = 2\pi\,\delta(\Omega - \Omega'),$$
 (2.8b)

and analogous expressions apply to the remaining noise operators.

Substituting Eqs. (2.5) and (2.6) into the equations of motion (2.2), retaining only the terms linear in the small perturbations, and applying the Fourier transform to the resulting expressions yield the following coupled algebraic equations:

$$(\gamma_{+} - i\Omega)c_{+}(\Omega) = -\eta_{+}C_{0}d(\Omega) + \sqrt{2\gamma_{+}} a_{+}(\Omega) \quad (2.9a)$$

$$(\gamma_{-} - i\Omega)c_{-}(\Omega) = \eta_{-}C_{0}d^{\dagger}(-\Omega) + \sqrt{2\gamma_{-}} a_{-}(\Omega) \quad (2.9b)$$

$$(\gamma_{m} - i\Omega)d(\Omega) = C_{0}\left[\eta_{-}c_{-}^{\dagger}(-\Omega) + \eta_{+}c_{+}(\Omega)\right] + \quad (2.9c)$$

$$+ \sqrt{2\gamma_{m}} \hat{q}(\Omega).$$

It follows from this set that the fluctuations of the optical mode near the central frequency ω_0 do not couple to the sideband modes at ω_{\pm} . Consequently, the equation governing the field component (2.2a) is dynamically independent and is omitted from further consideration.

We focus on the output field amplitudes b_{\pm} , which represent the measurable quantities of the system. In practice, these quantities can be accessed experimentally using a balanced homodyne detection scheme. To facilitate the analysis, we define the amplitude and phase quadratures of the field operators as follows:

$$a_{\pm a} = \frac{a_{\pm}(\Omega) + a_{\pm}^{\dagger}(-\Omega)}{\sqrt{2}},$$
 (2.10a)

$$a_{\pm\phi} = \frac{a_{\pm}(\Omega) - a_{\pm}^{\dagger}(-\Omega)}{i\sqrt{2}}.$$
 (2.10b)

Using Eqs. (2.4), (2.9), and (2.10), we obtain the following expressions for the amplitude and phase quadratures of the output fields \hat{b}_{\pm} :

$$b_{\pm a} = (\xi_{\pm} \mp A_{\pm}) a_{\pm a} \mp B a_{\mp a} \mp F_{\pm} \sqrt{2\gamma_m} q_a, \quad (2.11a)$$

$$b_{\pm\phi} = (\xi_{\pm} \mp A_{\pm}) a_{\pm\phi} \pm B a_{\mp\phi} - F_{\pm} \sqrt{2\gamma_m} q_{\phi}, \quad (2.11b)$$

where the coefficients are defined as

$$A_{\pm} = \frac{2\gamma_{\pm}\Gamma_{\pm}}{(\gamma_{\pm} - i\Omega)(\Gamma_m - i\Omega)}, \quad \xi_{\pm} = \frac{\gamma_{\pm} + i\Omega}{\gamma_{\pm} - i\Omega}, \quad (2.12a)$$

$$A_{+} = \xi_{+} - A_{+} = \xi_{+} \left(\frac{\gamma_{m} - \Gamma_{+}^{*} - \Gamma_{-} - i\Omega}{\Gamma_{m} - i\Omega} \right), (2.12b)$$

$$A_{-} = \xi_{-} + A_{-} = \xi_{-} \left(\frac{\gamma_{m} + \Gamma_{+} + \Gamma_{-}^{*} - i\Omega}{\Gamma_{m} - i\Omega} \right), (2.12c)$$

$$B = \frac{2}{\Gamma_m - i\Omega} \sqrt{\frac{\gamma_+ \gamma_- \Gamma_+ \Gamma_-}{(\gamma_+ - i\Omega)(\gamma_- - i\Omega)}},$$
 (2.12d)

$$F_{\pm} = \frac{1}{\Gamma_m - i\Omega} \sqrt{\frac{2\gamma_{\pm}\Gamma_{\pm}}{\gamma_{\pm} - i\Omega}},$$
 (2.12e)

$$\Gamma_{\pm} = \frac{\eta_{\pm}^2 C_0^2}{\gamma_+ - i\Omega}, \quad \Gamma_m = \gamma_m + \Gamma_+ - \Gamma_-, \tag{2.12f}$$

$$\Gamma_{m0} = \Gamma_m|_{\Omega=0} = \gamma_m + G_+ - G_-.$$
 (2.12g)

Here, Γ_{m0} represents the effective bandwidth of the mechanical oscillator, modified by the optical back action (nonlinear optical damping).

In the limiting case where $\Omega, \gamma_m \ll \gamma_{\pm}, (G_+ - G_-),$ Eqs. (2.11) can be simplified to

$$b_{\pm a} = \mp \mathcal{A}_{\pm} a_{\pm a} \mp B a_{\mp a} \mp F_{\pm} \sqrt{2\gamma_m} q_a, \qquad (2.13a)$$

$$b_{\pm\phi} = \mp \mathcal{A}_{\pm} a_{\pm\phi} \pm B a_{\mp\phi} - F_{\pm} \sqrt{2\gamma_m} q_{\phi}, \qquad (2.13b)$$

$$A_{\pm} \simeq \pm \frac{G_{+} + G_{-}}{G_{+} - G_{-}}, \quad B \simeq \frac{2\sqrt{G_{+}G_{-}}}{G_{+} - G_{-}},$$
 (2.13c)

$$F_{\pm} \simeq \frac{\sqrt{2G_{\pm}}}{G_{+} - G_{-}}.$$
 (2.13d)

The corresponding spectral density $S_{b\pm a}$ can then be estimated as

$$S_{b\pm} \simeq \frac{(G_+ + G_-)^2 + 4G_+G_-}{(G_+ - G_-)^2} + \frac{2G_\pm \gamma_m (2n_T + 1)}{(G_+ - G_-)^2}.$$
 (2.14)

It follows directly that $S_{b_{\pm a}} > 1$, indicating that each quadrature, when measured individually, exhibits a noise level exceeding the shot-noise limit. Same result is valid for $S_{b_{\pm \phi}} > 1$.

D. Continuous variable entanglement

The entanglement criterion based on the sum of dispersions, commonly referred to as the Duan–Simon entanglement criterion [9, 10], provides a rigorous measure of continuous-variable entanglement by evaluating the total dispersion of a pair of operators of Einstein-Podolsky-Rosen (EPR) type. For the analysis of our optomechanical system, we employ this criterion using a slightly modified set of EPR-like operators:

$$\hat{u} = \hat{x}_1 e^{i\phi_1} \cos \theta + \hat{x}_2 e^{i\phi_2} \sin \theta, \tag{2.15a}$$

$$\hat{v} = \hat{p}_1 e^{i\phi_1} \cos \theta - \hat{p}_2 e^{i\phi_2} \sin \theta. \tag{2.15b}$$

In this notation, the operators \hat{x}_j amd \hat{p}_j denote the quadrature operators of the two modes j=1,2, while the parameters θ_j and $\phi+j$ allow optimization of the relative weighting and phase of the quadratures. According to this criterion, a two-mode state is entangled if the sum of the dispersions of the operators \hat{u} and \hat{v} satisfies:

$$\langle (\Delta \hat{u})^2 \rangle + \langle (\Delta \hat{v})^2 \rangle < 1.$$
 (2.16)

Experimentally, the quadratures of the output fields b_{\pm} can be measured using a balanced homodyne detector, and their Fourier-domain amplitude and phase quadratures are given by Eq. (2.11). To verify whether the modes b_{\pm} are quantum-entangled, it is necessary to check that the inequality (2.16) holds. For many practical purposes, it is convenient to reformulate the criterion in terms of spectral densities rather than total dispersions. In this representation, the criterion can be expressed as:

$$S_{\alpha_a} + S_{\alpha_\phi} < 2. \tag{2.17}$$

for one-sided spectral densities S_{α_a} and S_{α_ϕ} of EPR-like variables

$$\alpha_a(\Omega) = a_{1a}(\Omega)e^{i\phi_1}\cos\theta + a_{2a}(\Omega)e^{i\phi_2}\sin\theta, \quad (2.18a)$$

$$\alpha_{\phi}(\Omega) = a_{1\phi}(\Omega)e^{i\phi_1}\cos\theta - a_{2\phi}(\Omega)e^{i\phi_2}\sin\theta.$$
 (2.18b)

The quadrature operators satisfy the canonical commutation relations:

$$[a_{1,2a}(\Omega), a_{1,2\phi}(\Omega')] = 2\pi\delta(\Omega - \Omega').$$
 (2.19)

If inequality (2.17) is satisfied for certain spectral frequencies Ω , this indicates that the two-mode system is in a quantum-entangled state. The spectral form of the criterion allows a direct analysis of frequency-dependent entanglement, which is particularly relevant for optomechanical systems where the quadratures a_{1a} , a_{2a} , $a_{1\phi}$, and $a_{2\phi}$, are naturally measured in the Fourier domain.

E. Entanglement detection

We propose to measure the amplitude quadratures b_{+a} and b_{-a} individually and then form their weighted linear combination to reveal the presence of entanglement between the two optical modes. Specifically, let us define a linear combination β_{a+} of the amplitude quadratures (c.f. (2.18)) as follows:

$$\beta_{a+} = z_+ b_{+a} + z_- b_{-a}, \tag{2.20}$$

$$|z_{+}|^{2} + |z_{-}|^{2} = 1 (2.21)$$

where $z_{\pm}(\Omega)$ are complex, frequency-dependent coefficients that can be adjusted in post-processing to minimize the single-sided spectral density $S_{\beta_{a+}}$ of β_{a+} . The normalization condition (2.21) ensures that for *uncorrelated* vacuum outputs b_{+a} and b_{-a} , one obtains $S_{\beta_{a+}} = 1$,

whereas for entangled outputs the spectral density drops below unity, $S_{\beta_{a+}} < 1$, within certain frequency ranges.

To satisfy the entanglement condition given by (2.17), it is also necessary that the spectral density of the phase quadrature combination $\beta_{\phi-} = z_-b_{+\phi} - z_+b_{-\phi}$ (see (2.18)) be smaller than unity. A straightforward calculation shows that for identical coefficients z_+ and z_- , the spectral densities of these two combinations are equal:

$$S_{\beta_{a+}} = S_{\beta_{\phi-}}. (2.22)$$

Therefore, to characterize the entanglement properties of the system, it suffices to evaluate only $S_{\beta_{a+}}$.

The optimal choice of the coefficients z_{\pm} is determined by the trade-off between two competing effects. On the one hand, the mechanical degree of freedom mediates the optical correlations responsible for quantum entanglement, so a large contribution from the mechanical quadrature d_a to β_{a+} enhances the entanglement. On the other hand, the thermal noise associated with the mechanical oscillator is typically very strong $(n_T \gg 1)$. To suppress the influence of this noise, one should choose z_+ and z_- to be nearly equal in magnitude, which reduces the contribution of the thermal term q_a . As can be seen from the last term in (2.20), the part of β_{+a} proportional to the mechanical noise is

$$\beta_{+a}^{(q)} \simeq (F_{-}z_{-} - F_{+}z_{+})\sqrt{2\gamma_{m}}q_{a}.$$
 (2.23)

Thus, when $|z_{+}| \simeq |z_{-}|$, the term containing q_{a} is significantly reduced, which minimizes the impact of the thermal noise.

Assuming that the input fluctuations $a_{\pm a}$ correspond to vacuum noise, the spectral density of β_{a+} can be derived from Eqs. (2.11, 2.20) and expressed as follows:

$$S_{\beta_{a+}} = S_q + S_T, \tag{2.24a}$$

$$S_q = \left| A_+ z_+ + B z_- \right|^2 + \left| A_- z_- - B z_+ \right|^2, \quad (2.24b)$$

$$S_T = 2\gamma_m \left| -F_+ z_+ + F_- z_- \right|^2 \left(n_T + \frac{1}{2} \right), \quad (2.24c)$$

where S_q represents the contribution from quantum fluctuations and S_T accounts for the thermal noise of the mechanical oscillator.

Under the normalization condition (2.21), it is convenient to express z_+ and z_- in the parametric form:

$$z_{+} = e^{-i\phi_{+}} \sin \theta, \quad z_{-} = e^{-i\phi_{-}} \cos \theta,$$
 (2.25a)

$$\Rightarrow |z_{+}|^{2} = \sin^{2}\theta, |z_{-}|^{2} = \cos^{2}\theta,$$
 (2.25b)

$$z_{+}z_{-}^{*} = e^{-i\phi}\cos\theta\sin\theta, \quad \phi = \phi_{+} - \phi_{-}$$
 (2.25c)

$$z_{\perp}^* z_{-} = e^{i\phi} \cos\theta \sin\theta. \tag{2.25d}$$

This parametrization shows that only two independent parameters, θ and the relative phase $\phi = \phi_+ - \phi_-$, govern the linear combination of the output quadratures. The optimal values of these parameters, $\theta(\Omega)$ and $\phi(\Omega)$,

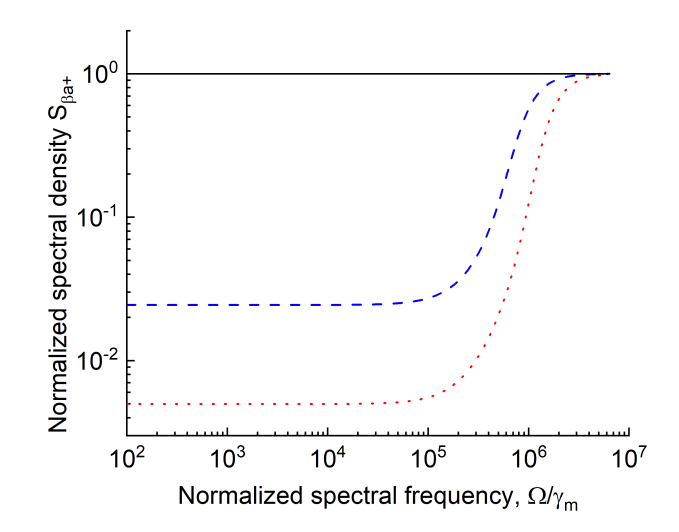


Figure 1. Spectral density $S_{\beta_{a+}}$ (2.24) as function of spectral frequency Ω . Solid black line stands for SQL. Dashed blue line stands for the input power P_{in} and other parameters from Table I, dotted red line corresponds to five time larger (×5) P_{in} . Parameters z_{\pm} are selected in the optimal way, parameter $G = (G_+ + G_-)/2 = 2 \times 10^6 \, \gamma_m$. $S_{\beta_{a+}}$ barely depends on opto-mechanical damping since $|G_+ - G_-| < 0.05 \, G$.

should be chosen such that the interference between correlated noise terms maximizes the suppression of $S_{\beta_{a+}}$.

For the simplest case,

$$\Omega = 0, \Rightarrow \xi_{\pm} = 1, \quad \Gamma_{\pm} = \Gamma_{\pm}^* = G_{\pm},$$
 (2.26)

one can derive the following approximation:

$$S_{\beta_{a+}}|_{\Omega=0}^{\min} \simeq \frac{\gamma_m^2 + (\sqrt{G+} - \sqrt{G_-})^4}{(\gamma_m + G_+ - G_-)^2} +$$
 (2.27a)

$$+\frac{\left(\sqrt{G_{+}}-\sqrt{G_{-}}\right)^{2}}{\Gamma_{m}}\left[\frac{2\gamma_{m}\left(n_{T}+\frac{1}{2}\right)}{\Gamma_{m}}\right] \qquad (2.27b)$$

The first term in Eq. (2.27) represents the contribution of optical vacuum fluctuations, while the second term corresponds to the thermal noise of the mechanical oscillator. The entanglement is possible when $G_+ - G_- \gg \gamma_m$.

Figure 1 shows the dependence of the minimal spectral density $S_{\beta_{a+}}$ obtained with complex parameters $z_{\pm}(\Omega)$ optimally selected in post-processing. The parameters used in the simulations are summarized in Table I. In this regime, the contribution of the thermal noise (2.27b) is limited by

$$S_{\beta_{a+}|\Omega=0}^{\text{Th}} \simeq \frac{2\gamma_m \left(n_T + \frac{1}{2}\right)}{\left(\sqrt{G_+} + \sqrt{G_-}\right)^2}.$$
 (2.28)

This term can be smaller than unity and, hence, the light in the system can be entangled $(S_{\beta_{a+}} + S_{\beta_{\phi-}} = 2S_{\beta_{a+}} < 2)$. This is the main observation of our study. The ultimate frequency bandwidth of the entanglement $\Delta\Omega_{ent}$ in

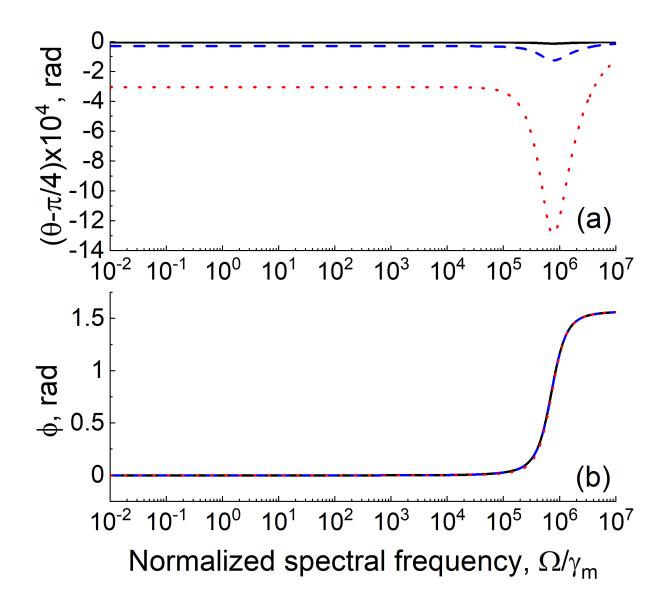


Figure 2. Optimal angles $\theta(\Omega)$ and $\phi(\Omega)$ defined in (2.25) as functions of spectral frequency Ω . The curve correspond to parameters $G=(G_++G_-)/2=2\times 10^6\,\gamma_m$ and $G_+-G_-=10^3\gamma_m$ (black solid line), $G_+-G_-=10^4\gamma_m$ (blue dashed line), $G_+-G_-=10^5\gamma_m$ (red dotted line). Other parameters are taken from Table I.

the case of optimally selected frequency dependent coefficients z_{\pm} can be defined as $S_{\beta_{a+}}(\Delta\Omega_{ent})=2S_{\beta_{a+}}|_{\Omega=0}^{\min}$. In a practically interesting case $n_T\gg 1$, $(G_+-G_-)\gg \gamma_m$, $0.05G\geq |G_+-G_-|$, and $\gamma_{\pm}=\gamma_0$, the bandwidth is determined primarily by the optical decay rate and is practically independent of the opto-mechanical damping value Γ_m

$$\Delta\Omega_{ent} \simeq \gamma_0.$$
 (2.29)

Plots for Fig. 1 are obtained for optimal angle θ and phase ϕ in (2.25), which in turn are functions of spectral frequency Ω . Their plots are presented on Fig. 2. We

Table I. Parameters of the silicon nitride membrane-based mechanical oscillator and the optical cavity employed in the numerical estimates.

| nericai estimates. | | |
|---|----------------------|------------------|
| Membrane | | |
| Mass, m | $5 \cdot 10^{-11}$ | kg |
| Frequency, $\omega_m/2\pi$ | $2 \cdot 10^{6}$ | $_{\mathrm{Hz}}$ |
| Quality factor $Q = \frac{\omega_m}{2\gamma_m}$ | $0.6 \cdot 10^{7}$ | |
| Temperature, T | 10 | Κ° |
| Thermal phonons number, n_T | $1.04 \cdot 10^5$ | |
| Cavity | | |
| Effective length of the cavity, L | 10 | $_{\rm cm}$ |
| Bandwidth, γ_0 | $3 \cdot 10^{5}$ | $ s^{-1} $ |
| Wave length, $\lambda = 2\pi c/\omega_0$ | $1.55 \cdot 10^{-6}$ | m |
| Input power P_{in} | 10^{-2} | W |
| Pump parameter $G = (G_+ + G)/2$ | $2.2 \cdot 10^{6}$ | s^{-1} |

see that angle θ slightly depends on Ω , while phase ϕ monotonically increases from zero to about $\pi/2$.

III. DISCUSSION

The primary goal of this paper is to provide proof-of-principle evidence for entanglement generation in a resonant optomechanical system. Using the parameter set listed in Table I, we numerically demonstrate that the system can operate in a regime where entanglement is produced reliably. These parameters satisfy the conditions

$$\gamma_m \ll G_+ - G_- \le \gamma_\pm, \qquad \gamma_0 \ll \omega_m, \qquad (3.1)$$

$$\frac{G_+ + G_-}{2} \gg n_T \gg 1,$$
 (3.2)

under which resonantly enhanced opto-mechanical interactions are most effective. Equations (3.1)–(3.2) ensure, respectively, (i) sufficiently strong and well-resolved sideband coupling, (ii) operation deep in the resolved-sideband regime, and (iii) dominance of coherent opto-mechanical rates over thermal decoherence.

It is worth noting, however, that although this parameter set demonstrates the feasibility of generating entanglement, additional optimization will be required for specific experimental implementations. Such optimization, aimed at maximizing the entanglement strength, robustness, and detection efficiency, will be discussed elsewhere.

A. Entanglement and oscillator temperature

In the framework of optomechanical generation of quantum-entangled states of light, we are interested exclusively in the case of a positive optical additive. In this regime, the quality factor of the mechanical oscillator can be significantly reduced, which in turn suppresses the amplitude of classical thermal noise that would otherwise hinder the establishment of entanglement.

Indeed, since the thermal occupation number $n_T\gg 1$, the second term in Eq. (2.27) dominates under typical experimental conditions. This thermal contribution can be reduced in two ways: (a) through parametric cooling, as the factor in square brackets reflects the effective reduction of the thermal noise number; and (b) by tuning the optical pump parameters such that $|z_+|\simeq |z_-|$, as discussed earlier in Eq. (2.23). As a result, operating with a positive optical additive to the mechanical attenuation enhances both the fidelity and robustness of the generated entangled states.

Depending on the sign of the optical additive G_+-G_- , the effective quality factor of the mechanical oscillator can either increase or decrease [31]. The optical damping decreases the mean number n_T' of thermal phonons:

$$n_T' \simeq \frac{\gamma_m}{|\Gamma_m|} n_T \simeq \frac{\gamma_m}{G_+ - G_-} n_T \ll n_T$$
 (3.3)

Therefore, the entanglement is observed when the oscillator is optically cooled.

In the case of symmetric opto-mechanical system, when $G_{+} = G_{-}$ no entanglement is generated. Physically, the entanglement is not produced since cooling of mechanical oscillator is not possible.

B. Distinction with the parametric entanglement

It is instructive to compare the performance of the conventional parametric entanglement source with that of the optomechanical source described here. To this end, let us consider a non-degenerate optical parametric amplifier. The amplifier is assumed to be implemented as a Fabry–Perot cavity containing a nonlinear $\chi^{(2)}$ crystal. An electromagnetic pump wave with amplitude E_0 and frequency $2\omega_0 = \omega_1 + \omega_2$ propagates through the crystal, where ω_1 and ω_2 are the resonant frequencies supported by the optical cavity.

The temporal evolution of the interacting optical modes can then be described by the following set of coupled equations:

$$\dot{\hat{c}}_1 + \gamma_1 \hat{c}_1 = G_{par} \hat{c}_2^{\dagger} + \sqrt{2\gamma_1} \hat{a}_1,$$
 (3.4a)

$$\dot{\hat{c}}_2 + \gamma_2 \hat{c}_2 = G_{par} \hat{c}_1^{\dagger} + \sqrt{2\gamma_2} \hat{a}_2.$$
 (3.4b)

Here \hat{c}_1 , \hat{c}_2 and \hat{a}_1 , \hat{a}_2 are operators of slow amplitudes of the intracavity and external optical fields (defined identically with 2.2 and 2.3), respectively. The parameter $G_{par} = \chi^{(2)} E_0$ stands for the parametric gain. The output field is found from expressions identical to (2.4).

Let us introduce the amplitude and phase quadratures of the electromagnetic fields:

$$a_a = \frac{a(\Omega) + a^{\dagger}(-\Omega)}{\sqrt{2}}, \quad a_{\phi} = \frac{a(\Omega) - a^{\dagger}(-\Omega)}{i\sqrt{2}}.$$
 (3.5)

and combinations of the quadratures $g_{-} = (b_{1a} - b_{2a})/\sqrt{2}$ and $g_{+} = (b_{1\phi} + b_{2\phi})/\sqrt{2}$. We find for g_{-}

$$g_{-} = \frac{(\sqrt{\gamma_{1}\gamma_{2}} - G_{par})^{2} - i\Omega(\gamma_{1} - \gamma_{2}) + \Omega^{2}}{(\gamma_{1} - i\Omega)(\gamma_{2} - i\Omega) - G_{par}^{2}} \frac{a_{1a}}{\sqrt{2}} - \frac{(\sqrt{\gamma_{1}\gamma_{2}} - G_{par})^{2} + i\Omega(\gamma_{1} - \gamma_{2}) + \Omega^{2}}{(\gamma_{1} - i\Omega)(\gamma_{2} - i\Omega) - G_{par}^{2}} \frac{a_{2a}}{\sqrt{2}}, \quad (3.6)$$

$$g_{+} = \frac{(\sqrt{\gamma_{1}\gamma_{2}} - G_{par})^{2} - i\Omega(\gamma_{1} - \gamma_{2}) + \Omega^{2}}{(\gamma_{1} - i\Omega)(\gamma_{2} - i\Omega) - G_{par}^{2}} \frac{a_{1\phi}}{\sqrt{2}} + \frac{(\sqrt{\gamma_{1}\gamma_{2}} - G_{par})^{2} + i\Omega(\gamma_{1} - \gamma_{2}) + \Omega^{2}}{(\gamma_{1} - i\Omega)(\gamma_{2} - i\Omega) - G_{par}^{2}} \frac{a_{2\phi}}{\sqrt{2}}. \quad (3.7)$$

The one-sided power spectral density of the combination g_{\pm} has the following form:

$$S_{g_{\pm}}(\Omega) = \frac{\left[\left(\sqrt{\gamma_{1}\gamma_{2}} - G_{par}\right)^{2} + \Omega^{2}\right]^{2} + \Omega^{2}\left(\gamma_{1} - \gamma_{2}\right)^{2}}{\left(\gamma_{1}\gamma_{2} - G_{par}^{2} - \Omega^{2}\right)^{2} + \Omega^{2}\left(\gamma_{1} + \gamma_{2}\right)^{2}}.$$

$$(3.8)$$

The minimum of this spectral density, i.e. the maximum entanglement, is achieved at $\Omega \to 0$. This minimum has the following form:

$$\min S_{g_{\pm}} = \left(\frac{\sqrt{\gamma_1 \gamma_2} - G_{par}}{\sqrt{\gamma_1 \gamma_2} + G_{par}}\right)^2. \tag{3.9}$$

The bandwidth of the entanglement is

$$\Delta\Omega_{\chi^{(2)}} \simeq \frac{4\gamma_1\gamma_2\sqrt{\min S_{g_{\pm}}}}{\gamma_1 + \gamma_2} \left(1 - \frac{4\gamma_1\gamma_2\sqrt{\min S_{g_{\pm}}}}{\left(\gamma_1 + \gamma_2\right)^2}\right). \tag{3.10}$$

One can see, that the larger is the entanglement, the smaller is the bandwidth of the entanglement. Interestingly, defining frequency dependent quadratures, similarly to (2.20), does not result in the modification of the bandwidth.

The bandwidth of the opto-mechanically induced entanglement (see Fig. 1) is not correlated with the minimum of the spectral density $S_{\beta_{a+}}$, which distinguishes this configuration from the conventional case of entanglement generated by a parametric amplifier. This feature highlights a unique regime of optomechanical entanglement, where broad bandwidth and strong quantum correlation can coexist.

C. Ideal vs synodyne detection

The measurement scheme presented above is hard to realize. To enable post-processing, one must separate the output fields corresponding to the modes ω_+ and ω_- , whose frequencies differ by $2\omega_m$ and also filter out the pump light. This frequency difference is small on the optical scale, making spectral separation experimentally challenging.

Here we propose a simpler method for detecting entanglement based on the so-called synodyne detection technique [29]. In this approach, the coefficients z_{\pm} cannot be chosen as complex functions with arbitrary spectral dependence on Ω ; instead, they must remain constant. Despite this restriction, the method still enables the observation of entanglement, while offering a much simpler experimental realization.

The local oscillator field E_{LO} of the synodyne detector contains two carrier frequencies:

$$E_{LO} = A_{+}e^{-i\omega_{+}t} + A_{-}e^{-i\omega_{-}t} + \text{conj.}$$
 (3.11)

We are interested in the slowly varying components of the difference photocurrent I, that is, in the terms oscillating at frequencies close to zero:

$$I \sim \left[A_{+}^{*} e^{i\omega_{+}t} + A_{-}^{*} e^{i\omega_{-}t} \right] \times \times \left(b_{+} e^{-i\omega_{+}t} + b_{0} e^{i\omega_{0}t} + b_{-} e^{-i\omega_{-}t} \right) + \text{conj.}$$
 (3.12)

The rapidly oscillating terms $\sim e^{\pm i\omega_m t}$ (associated with the mode b_0 at ω_0), $\sim e^{\pm 2i\omega_m t}$, and higher harmonics

should be omitted. Equation (3.12) can be simplified:

$$I \sim A_{+}^{*}b_{+} + A_{+}b_{+}^{\dagger} + A_{-}^{*}b_{-} + A_{-}b_{-}^{\dagger}$$
 (3.13)

Equation (3.13) demonstrates that when the local oscillator amplitudes are real, $A_{\pm} = A_{\pm}^*$, the detection measures a weighted sum $z_{+}b_{a+} + z_{-}b_{a-}$ with constant

real coefficients z_{\pm} . Conversely, when the local oscillator amplitudes are purely imaginary, $A_{\pm} = -A_{\pm}^*$, the measured observable corresponds to a weighted sum $(z_{+}b_{\phi+} + z_{-}b_{\phi-})$ with real coefficients z_{\pm} .

The spectral density of the sum β_{a+} defined in Eq. (2.20) can be written for the case of constant coefficients $z_{\pm} = 1/\sqrt{2}$ as follows:

$$S_{\text{syno}} = \frac{1}{2} \left| \frac{\gamma_m - \left(\sqrt{\Gamma_+^*} - \sqrt{\Gamma_-}\right)^2 - i\Omega + \Delta\sqrt{\Gamma_+^*\Gamma_-}}{\gamma_m + \Gamma_+ - \Gamma_- - i\Omega} \right|^2 + \frac{1}{2} \left| \frac{\gamma_m + \left(\sqrt{\Gamma_+} - \sqrt{\Gamma_-^*}\right)^2 - i\Omega - \Delta^*\sqrt{\Gamma_+\Gamma_-^*}}{\gamma_m + \Gamma_+ - \Gamma_- - i\Omega} \right|^2 + (3.14a)$$

$$+ \gamma_m \left[n_T + \frac{1}{2} \right] \left| \frac{-\sqrt{1 + \xi_+}}{\gamma_m + \Gamma_+ - \Gamma_- - i\Omega} \right|^2, \qquad \Delta = \sqrt{(1 + \xi_+^*)(1 + \xi_-)} - 2. \tag{3.14b}$$

The approximate expressions (2.27) and (2.28) derived for the spectral density of the noise when $\Omega \to 0$ remain valid for the synodyne case. However, the synodyne detection may have narrower detection bandwidth if compared with the ideal one. The phase ϕ defined in Eq. (2.25) cannot be optimally chosen in the case of synodyne measurement. Figure 3 shows the spectral density $S_{\rm syno}$ for several values of optical damping Γ_{m0} using the parameters listed in Table I. For comparison, the figure also includes the corresponding spectral density $S_{\beta_{a+}}$. It can be seen that the two spectral densities coincide at zero frequency, while their entanglement bandwidths differ. For $\Gamma_{m0} \simeq \gamma_0$, the bandwidths of $S_{\beta_{a+}}$ and $S_{\rm syno}$ are similar; however, when $\Gamma_{m0} \ll \gamma_0$, the bandwidth of $S_{\rm syno}$ becomes significantly narrower.

Let us estimate the bandwidth of the synodyne detection. The optimal phase in $S_{\beta_{a+}}$ is primarily determined by the mechanical susceptibility, which becomes smoother when Γ_{m0} increases due to increase of the optical damping. Consequently, the effective bandwidth of S_{syno} increases with opto-mechanical damping, illustrating the trade-off between experimental simplicity and optimal entanglement detection.

To define the measurement bandwidth $\Delta\Omega$ we demand $S_{\rm syno}(\Delta\Omega) = 2S_{\beta_a+}^{\rm Th}|_{\Omega=0}^{\rm min}$ which results in

$$\Delta\Omega_{\rm syno} \simeq \left(\sqrt{G_+} - \sqrt{G_-}\right) \sqrt{2\gamma_m \left(n_T + \frac{1}{2}\right)}.$$
 (3.15)

D. Improvement of a ponderomotive sensor

The configuration of the broadband variational measurement of a force [32] resembles the setup analyzed in this work. Namely, the pumping of the principal optical mode ω_0 and detection of the output quadratures of the radiation from modes ω_{\pm} , which are separated from the main mode by the frequency of the mechanical os-

cillator, $\omega_{\pm}=\omega_0\pm\omega_m$, allows removal of the quantum back action and broadband detection of a classical force, acting on the mechanical oscillator. For instance, one can detect the output amplitude quadratures $j_{\pm a}$ and form their combinations as $\delta_{a+}=\left(j_{+a}+j_{a-}\right)/\sqrt{2}$ and $\delta_{a+}=\left(j_{+a}-j_{-a}\right)/\sqrt{2}$ to perform the back action evading measurement. In the symmetric case $(\eta_+=\eta_-=\eta,\ \gamma_+=\gamma_-=\gamma)$ these combinations take the following form:

$$\delta_{a-} = \xi \, \epsilon_{a-}, \quad \xi = \frac{\gamma + i\Omega}{\gamma - i\Omega}, \quad \mathcal{K} \equiv \frac{4\gamma \, \eta^2 C_0^2}{\gamma^2 + \Omega^2}, \quad (3.16a)$$

$$\delta_{a+} = \xi \left(\epsilon_{a+} - \frac{\mathcal{K} \, \epsilon_{a-}}{\gamma_m - i\Omega} \right) -$$

$$- \frac{\sqrt{\xi \mathcal{K}}}{\gamma_m - i\Omega} \left(\sqrt{2\gamma_m} q_a + f_{s\,a} \right),$$

where $\epsilon_{a\pm}=(e_{+a}\pm e_{-a})/\sqrt{2}$ represent the combinations of the input amplitude quadratures e_{+a} and e_{-a} of the input fields for the modes ω_+ and ω_- , respectively. Operators q_a and $f_{s,a}$ denote the amplitude quadratures of thermal noise and the signal force acting on the mechanical oscillator, respectively.

In Eq. (3.16b), the back-action term is proportional to the normalized pump power \mathcal{K} , yet this contribution can be eliminated through post-processing. Specifically, by measuring both δ_{a+} and δ_{a-} simultaneously, one can completely suppress the back-action and analyze the combination

$$\delta_{meas} = \delta_{a+} + \frac{\mathcal{K} \, \delta_{a-}}{\gamma_m - i\Omega} =$$

$$= \xi \epsilon_{a+} - \frac{\sqrt{\xi \mathcal{K}}}{\gamma_m - i\Omega} \left(\sqrt{2\gamma_m} q_a + f_{sa} \right), \quad (3.17)$$

which is free from back-action noise. Consequently, the precision of the force measurement is determined solely by the input fluctuations ϵ_{a+} . In most cases, ϵ_{a+} de-

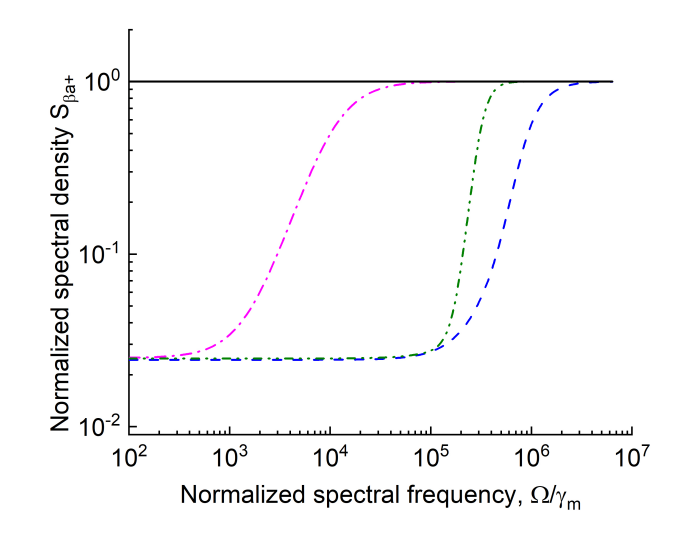


Figure 3. Spectral density $S_{\beta_{a+}}$ for the parameters listed in Table I. Black line represents SQL. Dashed blue line stands for the optimal detection procedure (c.f. Fig. 1) at $G/\gamma_m=2\times 10^6$, $(G_+-G_-)/\gamma_m=10^4$. The spectral density of the noise measured with the synodyne technique, $S_{\rm syno}$, given by Eq. (3.14), is shown by the dashed-dotted magenta line at the same parameters and the dashed-dotted-dotted green line at $G/\gamma_m=2\times 10^6$, $(G_+-G_-)/\gamma_m=\gamma_0/\gamma_m=3\times 10^5$

scribes quantum vacuum fluctuations, whose power spectral density equals unity $S_{\epsilon_{a+}}=1.$

The output radiation of the configuration discussed in this paper can be directly coupled to the input of the broadband variational measurement scheme. This corresponds to

$$e_{\pm} = b_{\pm}, \quad \Rightarrow \quad \epsilon_{a+} = \beta_{a+}, \tag{3.18}$$

leading to a substantially reduced spectral density:

$$S_{\epsilon_{a+}} = S_{\beta_{a+}} \ll 1. \tag{3.19}$$

In this manner, the sensitivity of the broadband variational measurement can be further enhanced.

It should be clarified that in Eq. (2.20) the coefficients z_{\pm} are complex and depend on the spectral frequency Ω , which, in general, prevents a straightforward substitution as in Eq. (3.18). However, in synodyne detection (considered previously in subsection III.C), the detected signal corresponds to a proportional combination (2.20) with a constant coefficient $z_{\pm} = 1/\sqrt{2}$ (at the cost of a narrower bandwidth — see Fig. 3). This demonstrates that the substitution (3.18) indeed represents a two-photon squeezing process with a spectral density significantly below unity, as expressed by Eq. (3.19).

E. Stability

The discussed opto-mechanical configuration is stable for the case of zero optical detuning even when $G \gg 1$,

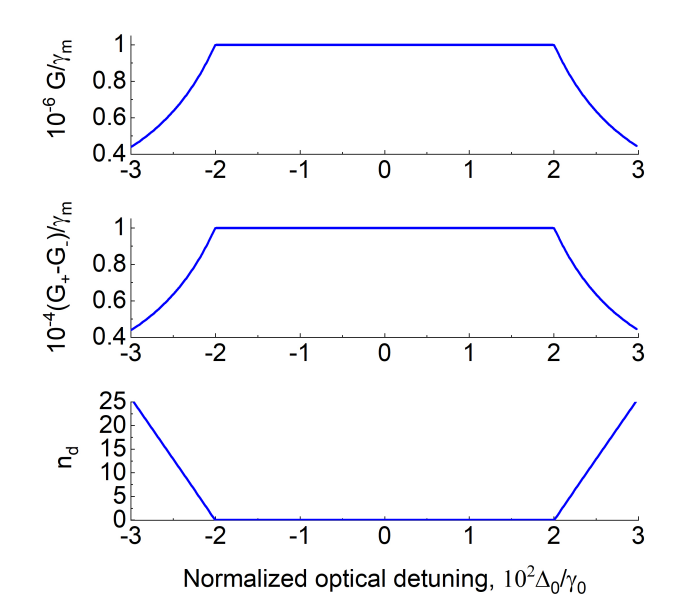


Figure 4. Parameters G, $G_+ - G_-$, and expectation value of the mechanical phonon number n_d found numerically for various values of the frequency detuning Δ_0 of the pump light from the corresponding optical mode. The system is stable when $|\Delta_0|/\gamma_0 < 2 \times 10^{-2}$.

but $G_+ > G_-$. However, introduction of nonzero detuning Δ_0 of the pump from the corresponding mode results in instability. We studied the stability of the system solving numerically set (2.2) for the numerical parameters listed in Table I and found that the stability region exceeds the frequency bandwidth of the mechanical mode. The numerical simulation was performed by selecting the detuning value and solving the nonlinear set of equations integrating them till the steady state solution is reached. The result of simulation means that the instability can be avoided by locking the pump laser to the corresponding optical mode. The results of simulations are illustrated by Fig. 4. It confirms practical viability of our proposal.

IV. CONCLUSION

We investigated optomechanical entanglement between optical modes that interact via a mechanical oscillator and analyzed the feasibility of experimentally observing this quantum correlation. The main challenge arises from equilibrium thermal noise affecting the mechanical subsystem. On one hand, thermal fluctuations must be suppressed; on the other, the quantum correlations produced by the optomechanical interaction must be preserved. We demonstrate that these requirements can be simultaneously satisfied in a realistic experimental configuration, enabling both the generation and detection of optomechanical entanglement. Achieving this regime requires careful engineering of the optomechanical coupling such that the mechanical oscillator is effectively cooled while

maintaining its nonlinear response that mediates entanglement. Compared to a conventional resonant parametric oscillator in the classical regime, the optomechanical architecture enables the generation of entangled optical modes over a significantly broader spectral bandwidth, assuming an equivalent entanglement strength. The resulting entangled light can enhance the sensitivity of optomechanical and electro-optical sensors and measurement systems.

of Moscow State University "Fundamental and Applied Space Research" and by the TAPIR GIFT MSU Support of the California Institute of Technology. The reported here research performed by ABM was carried out at the Jet Propulsion Laboratory, California Institute of Technology, under a contract with the National Aeronautics and Space Administration (80NM0018D0004). This document has LIGO number ??????.

ACKNOWLEDGMENTS

The research of AVK and SPV has been supported by the Interdisciplinary Scientific and Educational School

- A. Einstein, B. Podolsky, and N. Rosen, "Can quantum-mechanical description of physical reality be considered complete?," Phys. Rev., vol. 47, pp. 777–780, 1935.
- [2] E. Schrödinger, "Discussion of probability relations between separated systems," Proc. Cambridge Philos. Soc., vol. 31, pp. 555–563, 1935.
- [3] J. S. Bell, "On the einstein podolsky rosen paradox," Physics Physique Fizika, vol. 1, pp. 195–200, 1964.
- [4] A. Aspect, J. Dalibard, and G. Roger, "Experimental test of bell's inequalities using time-varying analyzers," <u>Phys.</u> Rev. Lett., vol. 49, pp. 1804–1807, 1982.
- [5] A. Aspect, P. Grangier, and G. Roger, "Experimental realization of einstein-podolsky-rosen-bohm gedankenexperiment: A new violation of bell's inequalities," <u>Phys.</u> <u>Rev. Lett.</u>, vol. 49, pp. 91–94, 1982.
- [6] P. G. Kwiat, A. M. Steinberg, and R. Y. Chiao, "High-visibility interference in a bell-inequality experiment for energy and time," Phys. Rev. A, vol. 47, no. 4, pp. R2472–R2475, 1993.
- [7] R. Horodecki, P. Horodecki, M. Horodecki, and K. Horodecki, "Quantum entanglement," <u>Rev. Mod.</u> Phys., vol. 81, pp. 865–942, 2009.
- [8] S. L. Braunstein and P. van Loock, "Quantum information with continuous variables," <u>Rev. Mod. Phys.</u>, vol. 77, pp. 513–577, 2005.
- [9] L.-M. Duan, G. Giedke, J. I. Cirac, and P. Zoller, "Inseparability criterion for continuous variable systems," <u>Phys.</u> Rev. Lett., vol. 84, pp. 2722–2725, 2000.
- [10] R. Simon, "Peres-horodecki separability criterion for continuous variable systems," <u>Phys. Rev. Lett.</u>, vol. 84, pp. 2726–2729, 2000.
- [11] M. D. Reid, "Demonstration of the einstein-podolskyrosen paradox using nondegenerate parametric amplification," Phys. Rev. A, vol. 40, pp. 913–923, 1989.
- [12] Z. Y. Ou, S. F. Pereira, H. J. Kimble, and K. C. Peng, "Realization of the einstein-podolsky-rosen paradox for continuous variables," <u>Phys. Rev. Lett.</u>, vol. 68, pp. 3663– 3666, 1992.
- [13] V. Josse, A. Dantan, A. Bramati, M. Pinard, and E. Giacobino, "Generation of two-color entangled light using a single laser," Phys. Rev. Lett., vol. 92, p. 123601, 2004.
- [14] B. Julsgaard, A. Kozhekin, and E. S. Polzik, "Experimental long-lived entanglement of two macroscopic objects,"

- Nature, vol. 413, pp. 400–403, 2001.
- [15] M. Aspelmeyer, T. J. Kippenberg, and F. Marquardt, "Cavity optomechanics," <u>Rev. Mod. Phys.</u>, vol. 86, pp. 1391–1452, 2014.
- [16] D. Vitali, S. Gigan, A. Ferreira, H. R. Böhm, P. Tombesi, A. Guerreiro, V. Vedral, A. Zeilinger, and M. Aspelmeyer, "Optomechanical entanglement between a movable mirror and a cavity field," <u>Phys. Rev. Lett.</u>, vol. 98, p. 030405, 2007.
- [17] S. Mancini, V. Giovannetti, D. Vitali, and P. Tombesi, "Entangling macroscopic oscillators exploiting radiation pressure," Phys. Rev. Lett., vol. 88, p. 120401, 2002.
- [18] R. Riedinger, A. Wallucks, I. Marinković, C. Löschner, M. Aspelmeyer, S. Hong, and S. Gröblacher, "Remote quantum entanglement between two micromechanical oscillators," Nature, vol. 556, pp. 473–477, 2018.
- [19] R. Ockeloen-Korppi, E. Damskägg, J.-M. Pirkkalainen, T. T. Heikkilä, F. Massel, and M. A. Sillanpää, "Stabilized entanglement of massive mechanical oscillators," Nature, vol. 556, pp. 478–482, 2018.
- [20] S. Pirandola, S. Mancini, D. Vitali, and P. Tombesi, "Entanglement transfer and rephasing in quantum networks," Phys. Rev. A, vol. 68, p. 062317, 2003.
- [21] C. Genes, A. Mari, D. Vitali, and P. Tombesi, "Robust entanglement of a micromechanical resonator with output optical fields," Phys. Rev. A, vol. 78, p. 032316, 2008.
- [22] A. H. Safavi-Naeini, S. Gröblacher, J. T. Hill, J. Chan, M. Aspelmeyer, and O. Painter, "Squeezed light from a silicon micromechanical resonator," <u>Nature</u>, vol. 500, pp. 185–189, 2013.
- [23] T. P. Purdy, P.-L. Yu, R. W. Peterson, N. S. Kampel, and C. A. Regal, "Strong optomechanical squeezing of light," Phys. Rev. X, vol. 3, p. 031012, 2013.
- [24] T. P. Purdy, K. E. Grutter, K. Srinivasan, and J. M. Taylor, "Optomechanical generation of squeezed light," <u>Science</u>, vol. 356, pp. 1265–1268, 2017.
- [25] Y.-D. Wang and A. A. Clerk, "Reservoir-engineered entanglement in optomechanical systems," <u>Phys. Rev.</u> Lett., vol. 110, p. 253601, 2013.
- [26] S. G. Hofer, W. Wieczorek, M. Aspelmeyer, and K. Hammerer, "Quantum entanglement and teleportation in pulsed cavity optomechanics," <u>Phys. Rev. A</u>, vol. 84, p. 052327, 2011.

- [27] M. R. Vanner, I. Pikovski, G. D. Cole, M. S. Kim, Č. Brukner, K. Hammerer, G. J. Milburn, and M. Aspelmeyer, "Pulsed quantum optomechanics," <u>Proc. Natl.</u> Acad. Sci. USA, vol. 108, pp. 16182–16187, 2011.
- [28] M. J. Woolley and A. A. Clerk, "Two-mode squeezed states in cavity optomechanics via engineering of a single reservoir," Phys. Rev. A, vol. 89, p. 063805, 2014.
- [29] L. Buchmann, S. Schreppler, J. Kohler, N. Spethmann, and D. Stamper-Kurn, "Complex Squeezing and Force Measurement Beyond the Standard Quantum Limit," Physical Review Letters, vol. 117, p. 030801, 2016.
- [30] H.J. Kimble, Y. Levin, A.B. Matsko, K.S. Thorne, and S.P. Vyatchanin, "Conversion of conventional gravitational-wave interferometers into QND interferometers by modifying input and/or output optics," Phys. Rev. D, vol. 65, p. 022002, 2001.
- [31] C. H. Metzger and K. Karrai, "Cavity cooling of a microlever," Nature, vol. 432, p. 1002–1005, 2004.
- [32] S. Vyatchanin, A. Nazmiev, and A. Matsko, "Broadband dichromatic variational measurement," <u>Physical Review</u> A, vol. 104, p. 023519, 2021.